Reprinted from The Journal of Physical Chemistry, 1995, 99.

Photofragment Imaging of Ozone Photodissociation: $O_3 \rightarrow O(^3P_j) + O_2(\tilde{X},v)$ at 226 nm

Jack A. Syage

The Aerospace Corporation, P.O. Box 92957, M5-754, Los Angeles, California 90009

Received: August 21, 1995; In Final Form: September 29, 1995[⊗]

We report photofragment angle-velocity distributions of the $O(^3P_{j=0,1,2})$ state for ozone photolysis at 226 nm in a time-of-flight mass spectrometer. A bimodal translational energy spectrum was recorded at 226 nm that peaked at internal energies of $O_2(X\,^3\Sigma_g,v)$ of $v = 15$ and 27, in general agreement with the measurements of Miller et al. [*Science* **1994**, *265*, 1831]. The yield of $O_2(v\geq 26)$ relative to total $O_2(X,v)$ is measured to be 0.06 by the $O(^3P)$ channel. This figure is important for evaluating a recently proposed explanation of the ozone deficit problem in the upper stratosphere. An anisotropy of $\beta = 1.2$ was measured for the high-velocity component corresponding to a M_y type transition and prompt dissociation. This is consistent with a pure $\tilde{B}^1B_2 \leftarrow \tilde{X}^1A_1$ transition.

Introduction

Ozone photolysis occurs primarily by singlet-state absorption and leads to the spin-allowed dissociation channels

$$O_3 + h\nu \rightarrow O_2(a^1\Delta_g) + O(^1D) \quad (1)$$

$$\rightarrow O_2(X^3\Sigma_g) + O(^3P) \quad (2)$$

The weak Chappius band absorption in the visible leads to reaction 2. The thermochemical threshold for reaction 1 occurs at 310 nm. The strong Hartley band in the ultraviolet correlates with reaction 1. The branching ratio of $O(^1D)/O(^3P)$ is about 0.90/0.10 for wavelengths short of 310 nm.[1]

Atmospheric models that calculate altitude-dependent ozone concentrations tend to underestimate the measured concentration of ozone in the upper stratosphere (40−70 km) by up to 20%.[2] This discrepancy, which has come to be known as the "ozone deficit problem", has stimulated much work to identify new sources of ozone that would bridge the gap.[3−7] A very intriguing hypothesis was recently proposed by Wodtke and co-workers[8−10] wherein highly vibrationally excited O_2, formed by O_3 photolysis (reaction 2), can re-form O_3 by the reaction

$$O_2(v \geq 26) + O_2 \rightarrow O_3 + O \quad (3)$$

Using stimulated emission pumping to prepare $O_2(v)$, Wodtke et al. showed that the rate of disappearance for $O_2(v)$ in collisions with O_2 increased sharply for $v \geq 26$, coincident with the thermochemical threshold for reaction 3.[8,9]

The importance of reaction 3 toward explaining the ozone deficit problem depends on the yield of $O_2(v\geq 26)$ formed by photolysis of ozone. This level of vibrational excitation can only occur by the $O(^3P)$ channel (reaction 2) and has a photochemical threshold for production of 243 nm. Whereas, solar radiation at this wavelength does not penetrate to the lower stratosphere, it can be important in the upper stratosphere where the ozone-deficit problem lies. The Houston and Wodtke groups used photofragment imaging to measure the $O(^3P_j)$ translational energy spectrum and observed a bimodal distribution for 226-nm photolysis, corresponding to $O_2(v)$ distributions peaking at $v = 14$ and $v = 27$.[10] They provided further evidence of a bimodal distribution from laser-induced fluorescence measurements of $O_2(v)$ from ozone photolysis.[10] On the basis of estimates of the relative yield of $O_2(v\geq 26)$, these investigators reasoned that reactions 2 and 3 can largely explain the ozone-deficit problem. As a counterpoint to the above discussion, Crutzen et al. recently reevaluated the ozone deficit problem and argued that the discrepancy disappears under new modeling conditions.[11] Nonetheless, the reaction sequence 2−3 is a potentially important source of ozone in the upper stratosphere that needs to be studied more thoroughly.

In this work we report photofragment angle-velocity distributions of the $O(^3P_{j=0,1,2})$ states for ozone photolysis at 226 nm by 2+1 REMPI in a time-of-flight mass spectrometer (TOFMS). Our method differs from previous translational energy measurements and imaging techniques in TOFMS in that a sectional image[12,13] as opposed to a projection image is recorded.[14,15] This approach provides direct measures of the differential cross section to photodissociation (within instrument angular resolution).

There have been several previous reports of ozone photodissociation studies by some form of photofragment translational energy spectroscopy. Fairchild et al. measured the O_2 translational energy spectrum for photolysis wavelengths between 270 and 310 nm and determined a $O(^1D)/O(^3P)$ branching ratio of about 0.90/0.10.[16] Sparks et al. obtained a similar branching ratio at 266 nm and also resolved the O_2 vibrational distribution for the major reaction channel 1 for 266-nm photolysis, but it was not possible to do the same for the weak reaction 2 because of overlapping signal.[17] In other work, translational energy measurements were reported using $O(^3P_j)$ detection. Kinugawa et al. measured the $O(^3P_j)$ translational energy spectrum by 2+1 REMPI in a TOFMS for 226-nm photolysis and observed a bimodal translational energy distribution.[18] However, they attributed the low-energy peak to dissociation of O_3 on their grids but did allow for the possibility that some of the yield could be due to some other process, such as a spin-forbidden mechanism. Their instrument angular resolution was not sufficient to resolve the anisotropy of the low-energy peak, a key measure that allowed Houston and co-workers to conclude that this component does not result from thermal or catalytic decomposition of ozone. Shamsuddin et al. measured $O(^3P_j)$ Doppler profiles by vacuum-ultraviolet laser-induced fluorescence for ozone photolysis at 266, 308, and 532 nm.[19] They reported anisotropy parameters and the branching ratios for the spin orbit components $j = 0$, 1, 2. Only average translational energy releases, rather than distributions, could be measured by this method. Also the photolysis energies were not suf-

[⊗] Abstract published in *Advance ACS Abstracts*, November 1, 1995.

0022-3654/95/2099-16530$09.00/0

ficiently high to test for low energy $O(^3P_j)$ peaks corresponding to energetic O_2. Most recently, Stranges et al. measured ozone photodissociation at 193 nm using high-resolution photofragment translational energy spectroscopy.[20] They identified several dissociation channels, almost all of which had negative β values. We discuss this observation later.

Experimental Section

Details of our experimental apparatus for measuring angle-velocity distributions have been described before.[12,13,21] Our time-of-flight (TOF) mass spectrometer consists of an ion optics assembly of three grids separated by 1 cm, a 1-m drift tube, and a 5-mm-diameter aperture mounted in front of an 18-mm diameter microchannel plate detector. Our experiment is based on the one-dimensional core TOF method.[22-24] The ionized fragment 3D spatial distribution expands as it travels down the drift tube (z axis) to the detector. The aperture placed in front of the detector limits the field-of-view to a cylinder of ions of maximum radial velocity $v_r = r/t_0$ where r is the effective aperture radius, and t_0 is the center of the ion TOF distribution. The angular and energy resolutions are dependent on photofragment speed v and are given, respectively by $\Delta\theta_z = \arcsin(v_r/v)$ and $\Delta v/v = 1 - (v_{z,\min}/v) = 1 - \cos\Delta\theta_z$. The detection cylinder limits the range of v_z that is observed for a particular v, thus defining the resolution $\Delta v/v$.

The results presented here were collected using 30 and 480 V/cm for the extraction and acceleration fields, respectively. Under these operating conditions, $t_0 = 15$ μs for O^+ ions. The z-component velocity is given by $v_z = F(t - t_0)/m$ where F is the extraction field and m is the fragment mass. The temporal resolution is 20 ns. A combination of the detector aperture diameter and blurring of the ion image due to diffraction off grids currently limits our spatial resolution to an effective aperture radius of about 4 mm, corresponding to a radial resolution of $v_r = 0.30$ km/s. 2D sectional photofragment images are obtained by recording a series of 1D core TOF spectra along a plane in the 3D photofragment velocity distribution. Displacement in the plane is achieved by moving the 3D ion packet across the detector aperture using a pair of deflector plates mounted just above the ion-optics assembly.[12,13]

Pump and probe excitation are from the same 5 ns laser pulse at 226 nm. $O(^3P_{0,1,2})$ were ionized by 2+1 resonance-enhanced multiphoton ionization (REMPI) through the two-photon transition $3p^3P_{0,1,2} \leftarrow 2p^3P_{0,1,2}$. The angle α of the pump laser polarization relative to the drift tube z-axis, was varied by rotating a combination of a double Fresnel–Rhomb and a Glan–Taylor polarizer. Laser pulse energies and focusing conditions were adjusted to avoid space charge repulsion. TOF spectra were collected in ion-counting mode using a multichannel scalar/averager (Stanford Research Systems SR430).

Ozone was produced in a commercial ozonator using ultrapure O_2 flow. The molecular beam pulsed valve was modified for these experiments in two ways: (1) Inlet and outlet gas ports were installed to allow a flowing sample. The transit time to the valve from the ozonator is about 10 s. The sample residence time in the valve is estimated to be about 0.5 s. The gaseous sample encounters only glass and Teflon material until reaching the valve, which consists of stainless steel and inert composite parts. (2) A cooling line was wrapped around the solenoid coil and backside of the valve. Cold N_2 gas from a liquid N_2 cylinder was used to prevent the pulsed valve from heating up above 40 °C. This level of cooling was sufficient to minimize thermal production of O atoms in the valve. The O atom TOF are attributable solely to O_3 photolysis. No O atom signal was observed in a pure flow of O_2 with the ozonator off.

Analysis

The differential cross section for photodissociation with respect to fragment speed v and recoil solid angle Ω is given by

$$\frac{d^2\sigma}{d\Omega\, dv} = \frac{d\sigma}{d\Omega}g(v) = \frac{\sigma}{4\pi}[1 + \beta P_2(\cos\alpha)\, P_2(\cos\theta_z)]g(v) \quad (4)$$

where θ_z is the polar angle with respect to the drift tube z axis, $d\Omega = 2\pi \sin\theta_z d\theta_z$ is the laboratory-frame solid angle, and α is the angle of the laser polarization axis ϵ relative to the z axis. The photofragment recoil angle relative to ϵ is given by $\theta = \theta_z - \alpha$. The second Legendre polynomial is defined as $P_2(x) = (3x^2 - 1)/2$ and β is the anisotropy factor for the angular distribution. The maximum anisotropy is given by the expression $\beta_{max} = 2P_2(\cos\chi)$, where is the angle χ between the bond breaking axis and the transition moment vector μ. The value of β approaches zero as the dissociation lifetime increases relative to the rotational period.

The flux of ions along the z axis per unit time and radial position for space focusing conditions has been reported elsewhere.[13,21,24] The observed TOF spectrum $I(v_z)$, integrated over the aperture size, is given by

$$I_\alpha(v_z) = \int_0^{v_r} \frac{d^2N}{dt\, dv_r'}\, dv_r' = \kappa \int_0^{v_r} \frac{d\sigma}{d\Omega}\frac{g(v)}{v^2} v_r'\, dv_r'$$

$$\approx \kappa \frac{v_r^2}{2v_z^2}\frac{d\sigma}{d\Omega_\alpha} g(v) \quad (5)$$

where κ encompasses a set of constants that includes laser intensity, molecular beam density, absolute photodissociation cross section, conversion constants, etc. Embedded in κ is the condition for space focusing, which holds that v_z is linear with t. Equation 5 describes 1D TOF spectra recorded through the center of the 3D velocity distribution for specific recoil angles α. The second line in eq 5 holds when $v_r \ll v$ and $g(v)$ is slowly varying over dv_r. In this limit $v \approx v_z$, in which case the product $v_z^2 I_\alpha(v_z)$, corresponds to the differential cross section for the molecular scattering angle $\theta = \alpha$. When $v_r \ll v$ is not satisfied, such as when v is small, v_z ceases to be a good measure of v. Then the integral in eq 5 must be carried out explicitly in order to fit a calculated $I_\alpha(v_z)$ to observed measurements. One method for fitting data is to take a trial $g(v)$ and calculate $I_\alpha(v_z)$ for individual increments of v and adding the results to obtain $I_\alpha(v_z)$.

The anisotropy parameter is obtained from the expression

$$\beta(v) = \frac{I_0(v_z) - I_{90}(v_z)}{0.5I_0(v_z) + I_{90}(v_z)} \quad (6)$$

The probability distribution for fragment translational energy is obtained from the relation $P(E)\, dE = g(v)\, dv$, which gives $P(E) = g(v)/mv$. The c.m. translational energy is computed from $E_{t,cm} = E_t M/(M - m)$ where m is the detected fragment mass and M is the molecular precursor mass. The internal energy of the O_2 fragment is determined from the conservation equation $E_{int} = h\nu - D_0 - E_{t,cm}$, where D_0 is the bond energy.

Results and Discussion

A 2D section of the 3D velocity distribution is presented in Figure 1 for the fragment $O(^3P_2)$. The ϵ vector is aligned along the drift-tube z axis. The most obvious feature in Figure 1 is

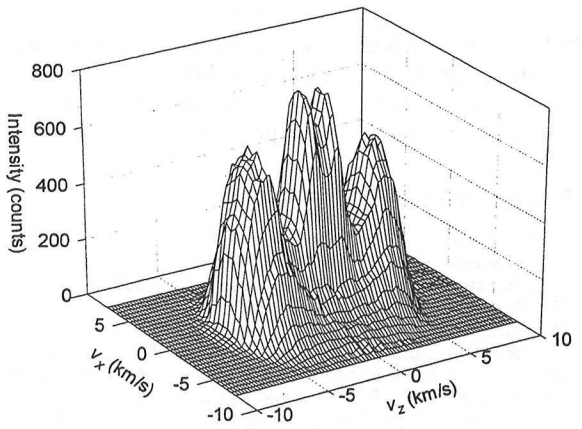

Figure 1. 2D photofragment image for $O(^3P_2)$ angle-velocity distribution at 226 nm. The laser polarization vector is aligned with the drift-tube axis ($\epsilon||z$).

a bimodal velocity distribution along ϵ. The high- and low-velocity components are both anisotropic, having maximum angular probabilities along ϵ. Photofragment images are useful for visualization of the angle-velocity distributions, however, for single-photon molecular photodissociation, the complete differential cross section can be determined from 1D $I_\alpha(v_z)$ spectra at $\alpha = 0$ and 90°.

$I_\alpha(v_z)$ TOF spectra are presented in Figure 2 for the $O(^3P_j)$ $j = 2$ and 1 fragment. There are three clear observables, (1) a bimodal velocity distribution is evident, (2) the bimodal distributions are highly peaked and anisotropic, and (3) the relative intensity of the lower velocity component decreases with j. These trends are also observed for $j = 0$. The higher velocity signal corresponds to the known $O_3 \rightarrow O(^3P_j) + O_2(X^3\Sigma_g^-)$ dissociation channel. It is formed in a relative yield of about 10:7:3 for $j = 2, 1, 0$, respectively. The high- and low-velocity distributions are similar to that observed by Miller et al.[10] The anisotropy parameter $\beta(v)$, calculated by eq 6, is plotted in Figure 2b,d. Equation 6 is valid only under core-sampling conditions; hence, the plot is terminated at low velocity at a value of $3v_r$ (where $v_r = 0.30$ km/s in these experiments).

For a $\tilde{B}^1B_2 \leftarrow \tilde{X}^1A_1$ transition, the transition moment lies along the molecular y axis, perpendicular to the C_{2v} axis and in-plane with the molecule. For a 116.7° bond angle,[25] one predicts a maximum anisotropy of $\beta = 1.17$. The observed fragment recoil anistropy $\beta(v)$ value for the high-velocity component in Figure 2 is the maximum allowable for an M_y type transition. This indicates a transition that is pure $\tilde{B}^1B_2 \leftarrow \tilde{X}^1A_1$ and a dissociation that is prompt with insignificant change in bond angle. Previous studies have stated lower β values. Fairchild reported values of $\beta \approx 1.2$ for the $O(^1D)$ channel, but $\beta \approx 0.5$ for $O(^3P)$ over the wavelength range 274−300 nm.[16] Kinugawa reported $\beta \approx 0.7$ for $O(^3P)$ at 226 nm, the same conditions as here.[18] Shamsuddin et al. measured $\beta = 0.81$ and 0.60 at 266 and 308 nm, respectively.[19] Interestingly, Stranges et al. reported the low value of $\beta = 0.09$ at 193 nm.[20] The reasons for the differences are not clear; however, the highly peaked velocity distribution for the fast component argues for a direct dissociation that should have a large anisotropy. Stranges et al. agree that dissociation is prompt but postulate that the bond angle decreases rapidly during dissociation to account for a low β value at 193 nm. We find no evidence for such dynamics at 226 nm for the high-velocity component.

The anistropy $\beta(v)$ at low velocity is significantly less than the value of $\beta = 1.2$ measured for the high-velocity component. A value of β ranging from 0.4 to 0.7 is measured for the low-velocity component depending on spin−orbit state j. As fragment velocity decreases, core sampling conditions become less valid, and evaluation of β by eq 6 deviate in a direction that understates the true values. Nonetheless, the peak of the low velocity component is at about $4v_r$ (where $v_r = 0.3$ km/s), which is in the strong core sampling limit. Therefore, we conclude that the decrease in β with v is a real effect. Electronic angular momentum of the $O(^3P_j)$ state due to the spin-orbit splitting may also have an effect on the measured β values, if an atomic alignment due to j-polarization occurs ($\mathbf{v}-\mathbf{j}$ correlation). The shape of the $\beta(v)$ curve for $j = 0$, where alignment is zero, is similar to that for $j = 1$ and $j = 2$ in Figure 2. However, the magnitude of the β is smaller by about 20% for $j = 0$. In future experiments, we plan to investigate the issue of j polarization and to record β values at lower fragment velocity under higher resolution conditions.

The dissociative potentials leading to the slow $O(^3P_j)$ components are not known. The dissociation of O_3 to $O(^3P) + O_2(^1D)$ is not a likely explanation because the process is spin forbidden and does not predict the observed shift in $O(^3P)$ translational energy. Furthermore, Miller et al. directly mea-

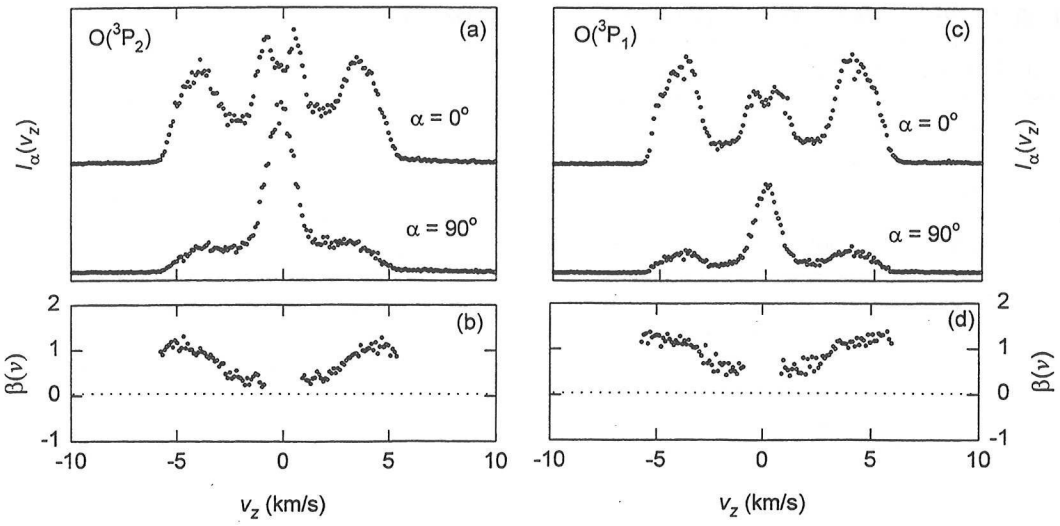

Figure 2. Angle-resolved $O(^3P_j)$ photofragment velocity distributions $I_\alpha(v_z)$ and velocity dependent anisotropy $\beta(v)$ for O_3 excitation at 226 nm where α is the alignment of ϵ relative to the drift-tube z axis. (a), (b) $j = 2$; (c), (d) $j = 1$. The time scale for the TOF spectra is $t_0 = 15.1$ μs and $2|t - t_0| = 550$ ns for the outer peak onsets.

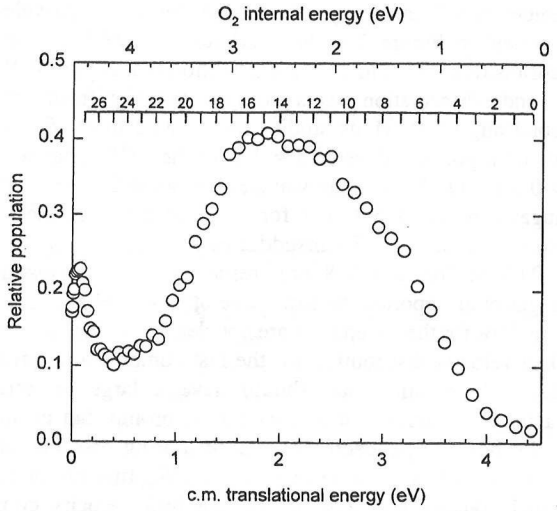

Figure 3. c.m. translational energy distribution for $O_3 \rightarrow O(^3P_j) + O_2$ photodissociation at 226 nm. The results are averaged over the relative yields of the $j = 0, 1, 2$ spin−orbit states.

sured a $O_2(v)$ distributions for $v = 19-26$ that shows a minimum at $v = 22$.[10] Xantheas et al. have calculated potential energy surfaces of ozone as a function of dissociation coordinate (C_s symmetry) and bond angle (C_{2v} symmetry).[26] They observe the excited state B_2-A_2 crossing but then find that the A_2 state crosses with the ground A_1 state (both A′ in C_s symmetry) at smaller bond angles. The transition state has a ring structure that can either open or eject an O atom. Such a mechanism could explain a lower β value due to the decreased bond angle and the possible ejection of the central oxygen atom.

One of the purposes of this work was to test the premise by Miller et al.[10] that the production of $O_2(v \geq 26)$ may explain the ozone deficit problem. In that regard, we have verified the presence of the slow $O(^3P)$ component observed by Miller et al. and have measured the relative yield of slow vs fast O atoms. The peak in the vibrational distributions for 226 nm photolysis in Figure 2 occurs at $v = 15$ and $v = 27$, in general agreement with Miller et al. The fraction $O_2(v \geq 26)$ to total $O_2(X,v)$ by the $O(^3P)$ channel at 226 nm is measured to be 0.055 ± 0.020, which compares to the value of 0.081 reported by Miller et al. Further work is needed to measure the yield of vibrationally excited O_2 at other wavelengths and to determine the potential energy surface that leads to the low translational energy dissociative limit.

Acknowledgment. I wish to thank Prof. P. L. Houston for valuable discussions and for communicating unpublished results. I also thank Dr. S. M. Beck for the loan of the SR430 and accompanying software. This work was supported by the Aerospace Sponsored Research program.

References and Notes

(1) (a) Wayne, R. P. *J. Geophys. Res.* **1993**, *98*, 13119. (b) Wayne, R. P. *Atmos. Environ.* **1987**, *21*, 1683, and references therein.
(2) Eluszkiewicz, J.; Allen, M. *J. Geophys. Lett.* **1993**, *98*, 1069.
(3) Slanger, T. G. *Science* **1994**, *265*, 1817.
(4) Gill, E. K.; Laidler, K. J. *Can. J. Chem.* **1958**, *36*, 79.
(5) Frederick, J. E.; Cicerone, R. J. *J. Geophys. Res.* **1985**, *90*, 10733.
(6) (a) Saxon, R. P.; Slanger, T. G. *J. Geophys. Res.* **1986**, *91*, 9877. (b) Simonaitis, R.; Leu, M. T. *Geophys. Res. Lett.* **1985**, *12*, 829.
(7) (a) Slanger, T. G.; Jusinski, L. E.; Black, G.; Gadd, G. E. *Science* **1988**, *241*, 945. (b) Park, H.; Slanger, T. G. *J. Chem. Phys.* **1994**, *100*, 287.
(8) Price, J. M.; Mack, J. A.; Rogaski, C. A.; Wodtke, A. M. *Chem. Phys.* **1993**, *175*, 83.
(9) Rogaski, C. A.; Price, J. M.; Mack, J. A.; Wodtke, A. M. *Geophys. Res. Lett.* **1993**, *20*, 2885.
(10) Miller, R. L.; Suits, A. G.; Houston, P. L.; Toumi, R.; Mack. J. A.; Wodtke, A. M. *Science* **1994**, *265*, 1831.
(11) Crutzen, P. J.; Gross, J.-U.; Bruhl, C.; Muller, R.; Russell III, J. M. *Science* **1995**, *268*, 705.
(12) Hertz, R. A.; Syage, J. A. *J. Chem. Phys.* **1994**, *100*, 9265.
(13) Syage, J. A. *Chem. Phys.*, submitted.
(14) (a) Chandler, D. W.; Houston, P. L. *J. Chem. Phys.* **1987**, *87*, 1445. (b) Chandler, D. W.; Thoman, Jr., J. W.; Janssen, M. H. M.; Parker, D. H. *Chem. Phys. Lett.* **1989**, *156*, 151.
(15) Bontuyan, L. S.; Suits, A. G.; Houston, P. L.; Whitaker, B. J. *J. Phys. Chem.* **1993**, *89*, 1443.
(16) Fairchild, C. E.; Stone, E. J.; Lawrence, G. M. *J. Chem. Phys.* **1978**, *69*, 3632.
(17) Sparks, R. K.; Carlson, L. R.; Shobatake, K.; Kowalczyk, M. L.; Lee, Y. T. *J. Chem. Phys.* **1980**, *72*, 1401.
(18) Kinugawa, T.; Sato, T.; Arikawa, T.; Matsumi, Y.; Kawasaki, M. *J. Chem. Phys.* **1990**, *93*, 3289.
(19) Shamsuddin, S. M.; Inagaki, Y.; Matsumi, Y.; Kawasaki, M. *Can. J. Chem.* **1994**, *72*, 637.
(20) Stranges, D.; Yang, X.; Chesko, J. D.; Suits, A. G. *J. Chem. Phys.* **1995**, *102*, 6067.
(21) Syage, J. A. *Chem. Phys. Lett.*, in press.
(22) Spiglanin, T. A.; Chandler, D. W. *Chem. Phys. Lett.* **1987**, *141*, 428.
(23) Ogorzalek Loo, R.; Haerri, H.-P.; Hall, G. E.; Houston, P. L. *J. Chem. Phys.* **1989**, *90*, 4222.
(24) Hwang, H. J.; Griffiths, J.; El-Sayed, M. A. *Int. J. Mass Spectrom. Ion Proc.* **1994**, *131*, 265.
(25) Herzberg, G. *Molecular Spectra and Molecular Structure;* Van Nostrand: New York, 1966.
(26) Xantheas, S. S.; Atchity, G. J.; Elbert, S. T.; Ruedenberg, K. *J. Chem. Phys.* **1991**, *94*, 8054.

JP952432F